Applied Catalysis B: Environmental 211 (2017) 98–105

Contents lists available at ScienceDirect

Applied Catalysis B: Environmental

journal homepage: www.elsevier.com/locate/apcatb

Structure defects assisted photocatalytic H_2 production for polythiophene nanofibers

Xupeng Zong[a,b,c], Xiang Miao[a,b,c], Shixin Hua[c], Li An[c], Xiang Gao[a,b,c], Wenshuai Jiang[c], Dan Qu[a,b,c], Zhijun Zhou[d,*], Xingyuan Liu[a], Zaicheng Sun[c,*]

[a] State Key Laboratory of Luminescence and Applications Changchun Institute of Optics, Fine Mechanics Physics, Changchun, 130033 Jilin, PR China
[b] University of Chinese Academy of Sciences, Beijing 100000, PR China
[c] Beijing Key Laboratory of Green Catalysis and Separation Department of Chemistry and Chemical Engineering School of Environmental and Energy, Beijing University of Technology, 100 Pingleyuan, Changyang District, Beijing 100124, PR China
[d] Institute of Nuclear Physics and Chemistry, China Academy of Engineering Physics, 64 Mianshan Road, Mianyang, Sichuan 621000, PR China

ARTICLE INFO

Article history:
Received 5 February 2017
Received in revised form 6 April 2017
Accepted 10 April 2017
Available online 13 April 2017

Keywords:
Photocatalytic H_2 production
Conjugated polymer
Polythiophene
Structural defects
Visible light response

ABSTRACT

Conjugated polymers (CPs) have been demonstrated to be excellent solar energy conversion materials, however, it is considered that pure CPs are not able to photocatalyze water splitting because of the fast recombination of photogenerated charge carriers. Here, we found polythiophene (PTh) nanofibrous structure can have a decent photocatalytic activity (2.19 mmol h^{-1} g^{-1}) and stability in ascorbic acid aqueous solution under visible light irradiation. Furthermore, PTh synthesized at high temperature will introduce structure defects, such as, α–β' coupling and end groups, which are beneficial to the charge separation. In addition, PTh synthesized at low temperature has long polymer chain and ordered arrangement of chain, which enhanced the light adsorption. Considering both light adsorption and charge separation, PTh compound nanostructure was rationally designed, PTh synthesized at low temperature as core to obtain good light adsorption and PTh prepared at high temperature as sheath to form more structure defects to promote charge separation. This PTh compound nanostructure exhibit higher photocatalytic H_2 production performance (2.8 mmol h^{-1} g^{-1}). Our finding may open a door for conjugated polymer for photocatalyst.

The photocatalytic splitting of water into hydrogen and oxygen using solar energy is a potentially clean and renewable source for hydrogen fuel. Many efforts have been made to develop photocatalyst with visible light response, like doped wide band gap semiconductors [1–3], which are still suffering from poor light absorption in the visible light. It is highly desired to explore narrow band gap semiconductors such as CdS, which has relatively wide band gap (2.4 eV) and poor stability [4,5]. On the other hand, the absorption coefficient of most inorganic semiconductor is lower than that of organic materials. Organic materials have their unique advantages, for example, tunable band gap via molecular structure, high absorption coefficient. However, limited research on the organic photocatalyst for water splitting has been carried out. Since 2009, g-C_3N_4 was discovered as a photocatalyst for H_2 production, only a few organic photocatalysts were explored, such as doped poly(trazine imide) [6], heptazine network [7], poly(azomethine)s [8], hydrazone-based covalent organic frameworks [9], triazine-based frameworks [10], triphenyl-azine frameworks [11], an organic push–pull polymer network/rutile composite [12] and microporous conjugated polymers [13–15]. These recent development of various polymer photocatalysts for hydrogen evolution was reviewed in detail by X. Wang [16].

Linear conjugated polymers such as polythiophene (PTh), polypyrrole (PPy) and polyaniline (PAn), are rarely investigated as photocatalyst although they were studied 3 decades ago. In 1980s, poly(*para*-phenylene) (PPP) was reported and exhibited modest photocatalytic H_2 production activity under UV light and weak performance under visible light (λ > 400 nm) [17,18]. Recently, P3HT has been employed as a light adsorption material in a composite with g-C_3N_4 for H_2 production. Compared with g-C_3N_4, the photocatalytic performance of the composite has a great increase under visible light irradiation. However, P3HT, even loaded with Pt, by itself exhibited negligible H_2 production performance under λ > 400 nm [19]. Generally, pure CPs are not able to photocatalyze water splitting because of the fast recombination of photogenerated charge carriers. Nevertheless, they can be used as sensitizers

* Corresponding authors.
E-mail address: sunzc@bjut.edu.cn (Z. Sun).

http://dx.doi.org/10.1016/j.apcatb.2017.04.033
0926-3373/

for other photocatalysts [20]. Guo and coworkers also prepared PAn-CdS composites for photocatalytic H_2 evolution under visible light ($\lambda > 420$ nm) [21]. Both cases showed that conjugated polymer could promote the light adsorption and then transfer the excited electron into the photocatalyst to enhanced H_2 evolution process.

It is well known that it should consider both light adsorption and charge separation efficiency to achieve water splitting H_2 evolution. Taking the view of energy level diagram, it requires the conduction band (CB) of photocatalyst should be higher than hydrogen reduction potential. And enough energy difference between CB and NHE is needed to make excited electron transfer. Nanostructure, scarification agent and cocatalyst are considered as effective ways to promote charge separation by shortening the charge transfer distance from the generation site to the surface, consuming holes and making spatial charge separation. Recently, constructing a certain concentration of defects on the semiconductor will also promote charge separation [22–24]. PTh and derivatives with a band gap of 1.9–2.1 eV are typical light adsorption materials for organic photovoltaics for high charge mobility and photostability [25]. It is expected to be a good photocatalyst for H_2 production because LUMO position of PTh is much higher (~1.0 eV) than the potential of H_2 reduction. In this case, charge separation will be the critical issue to solve the photocatalytic activity of PTh.

Herein, PTh nanofibers were directly synthesized via oxidation polymerization and exhibited high H_2 evolution rate ($2.19\ mmol\ h^{-1}\ g^{-1}$) in $0.1\ mol\ L^{-1}$ ascorbic acid (AA) aqueous solution under visible light ($\lambda > 420$ nm). Polymerization temperature were studied and we found that PTh nanofibers synthesized at 20 °C showed the best photocatalytic activity. FTIR, Raman and ^{13}C NMR spectra also disclosed that the content of structure defects, such as, α, β'-coupling, short polymer chain and end unit, increased as increasing the reaction temperature. Photodeposition of Pt nanoparticles illustrates that the structure defects are beneficial to trap the photogenerated electron and promote the charge separation. PTh synthesized at high temperature possess more structure defects. UV–vis spectra illustrate that PTh prepared at low temperature has stronger adsorption at near 600 nm region, and this band, which stands for the ordered arrangement of polymer chains, blueshifts with the rising the reaction temperature. It indicates that PTh synthesized at low temperature has more order structure and less structure defects which results in better adsorption. On the basis of above results, we designed novel PTh compound nanofibers firstly polymerized at low temperature and then raise up reaction temperature. Compound PTh nanofibers have better adsorption PTh as core and more structure defects on the shell, which exhibit higher photocatalytic activity.

Prior to synthesis of PTh, P3HT was tested for H_2 production. However, its hydrogen evolution rate is very low in $1.5\ \mu mol\ h^{-1}$ for 300 mg of catalyst, which is close to previous report [26] (Fig. S1). To prevent PTh from aggregation and promote charge separation, nanostructural PTh were firstly synthesized via one-step oxidized polymerization in CH_3CN using unsubstituted thiophene as monomer. As shown in Fig. 1A and S2, typical morphology of as-prepared PTh exhibited fibrous nanostructure with about 30–50 nm in diameter. The nanofibrous structure will ensure that most of the photoexcited excitons can diffuse to the surface. UV photoelectron spectroscopy (UPS) is often employed to determine the highest occupied molecular orbital (HOMO) of organic semiconductor. Fig. S3 shows VB UPS spectrum of as-prepared PTh. HOMO energy level (0.72 eV *v.s.* NHE) can be calculated from the band edge of UPS spectra. PTh nanofibers displays a broad adsorption band in the visible light region between 400 and 650 nm (Fig. 1D). The optical band gap (~1.94 eV) of PTh can be roughly calculated from the absorption edge, based on the Kubelka–Munk function (Fig. 1B). Based on the HOMO and band gap, then the Lowest Unoccupied Molecular Orbital (LUMO) position can be estimated at −1.22 eV *v.s.* NHE. The energy level diagram of PTh is shown in the inset of Fig. 1B. It clearly shows that the LUMO of PTh nanofiber is higher than the potential of H_2 reduction.

Hydrogen evolution is a typical method to evaluate the photocatalytic activity of photocatalyst. The conditions of reaction were optimized. Firstly, the sacrificial agents were optimized from Na_2SO_3-Na_2S, triethanol amine (TEOA), methanol (MeOH) and ascorbic acid (AA) (Fig. S4). As sulfur-contained polymer, Na_2SO_3-Na_2S buffer solution was tested as sacrificial agent, the H_2 evolution rate of PTh is about $480\ \mu mol\ h^{-1}\ g^{-1}$. When MeOH and TEOA was used as sacrificial reagents, the H_2 evolution rate is close to the Na_2SO_3-Na_2S case. When AA was employed, H_2 evolution rate dramatically increases and reaches ~$2190\ \mu mol\ h^{-1}\ g^{-1}$, indicating that AA is an efficient sacrificial hole acceptor for the PTh photocatalyst. A similar result on the crucial role of AA has also been observed by other researchers in P3HT/C_3N_4 composite photocatalyst [27]. Furthermore, cocatalyst amounts were optimized by photodeposition Pt nanoparticles on the PTh nanowire. 1.0 wt% Pt on PTh gives the best H_2 evolution rate (Fig. S5). We compared the full spectrum and visible light ($\lambda > 420$ nm). Under full spectrum light irradiation, H_2 production rate slightly increase and is close to $2200\ \mu mol\ h^{-1}\ g^{-1}$ (Fig. S6). That indicates that the UV light has faint contribution on the photocatalytic performance of PTh, mainly because the adsorption of PTh is relative weak in the UV light region. The H_2 evolution rate only shows a slight decrease after 4 successive cycles and 20 h' visible light irradiation, indicating the conjugated polymer PTh is a relatively stable photocatalyst (Fig. 1C). Fig. 1D shows the dependence of H_2 evolution rate of PTh on the irradiation wavelength, which measured with 20 nm band width optical filter for 5 mg PTh sample. At short wavelength, it gives low H_2 production rate. H_2 production rate gradually increases with increasing wavelength and reaches to maximum when the irradiation wavelength is 550 nm. Later, the H_2 production rate decreases with the increase of wavelength. The change of H_2 evolution rate of PTh is consistent with its adsorption spectrum. It indicates that the H_2 production rate strongly depends on the adsorption of PTh. Although the H_2 production rate is quite low (~$0.4\ \mu mol\ h^{-1}$) at individual wavelength, the integration of the curve is $6.7\ \mu mol\ h^{-1}$, which is lower to the H_2 production rate of PTh (~$10\ \mu mol\ h^{-1}$) from Fig. 1C due to low transmittance of optical filters. Concerning PTh is an organic polymer, the stability of photocatalyst was studied. Compared with common non-metal g-C_3N_4 synthesized from urea at 550 °C according to Chen's report [28], PTh exhibits superior photocatalytic activity (Fig. S1). Based on the above results, it clearly illustrates that conjugated polymer PTh could be an excellent organic photocatalyst under suitable conditions. It should be point out the performance of C_3N_4 could be greatly improved by modification with different methods [29–38]. Concerning this fact, we expect further improvements of PTh on catalytic performance could also be achieved in the future.

PTh-n samples prepared at different temperature were investigate, where n stands for the temperature. Figs. 2B and S7 illustrate the photocatalytic performance of PTh-n nanofibers. The photocatalytic activity first increases and then decreases as the temperature increases. That implies that the photocatalytic activity of PTh may be related to polymerization temperature. Fig. 2A shows the schematic chemical polymerization route of PTh with α, α'-coupling and α, β'-coupling routes. Normally, α, α'-coupling is preferred to obtain highly conjugated polymer. To avoid the occurrence of α, β'-coupling, the reaction normally carried out at low temperature to lower the active energy. When the polymerization carried out at high temperature, it will increase the number of initial center, which may result in short polymer chain. It gives high energy to the system and lead to the side reaction, for example, α, β'-coupling. These structure defects may result in cutting down the conjugation length and affect the adsorption of polymer.

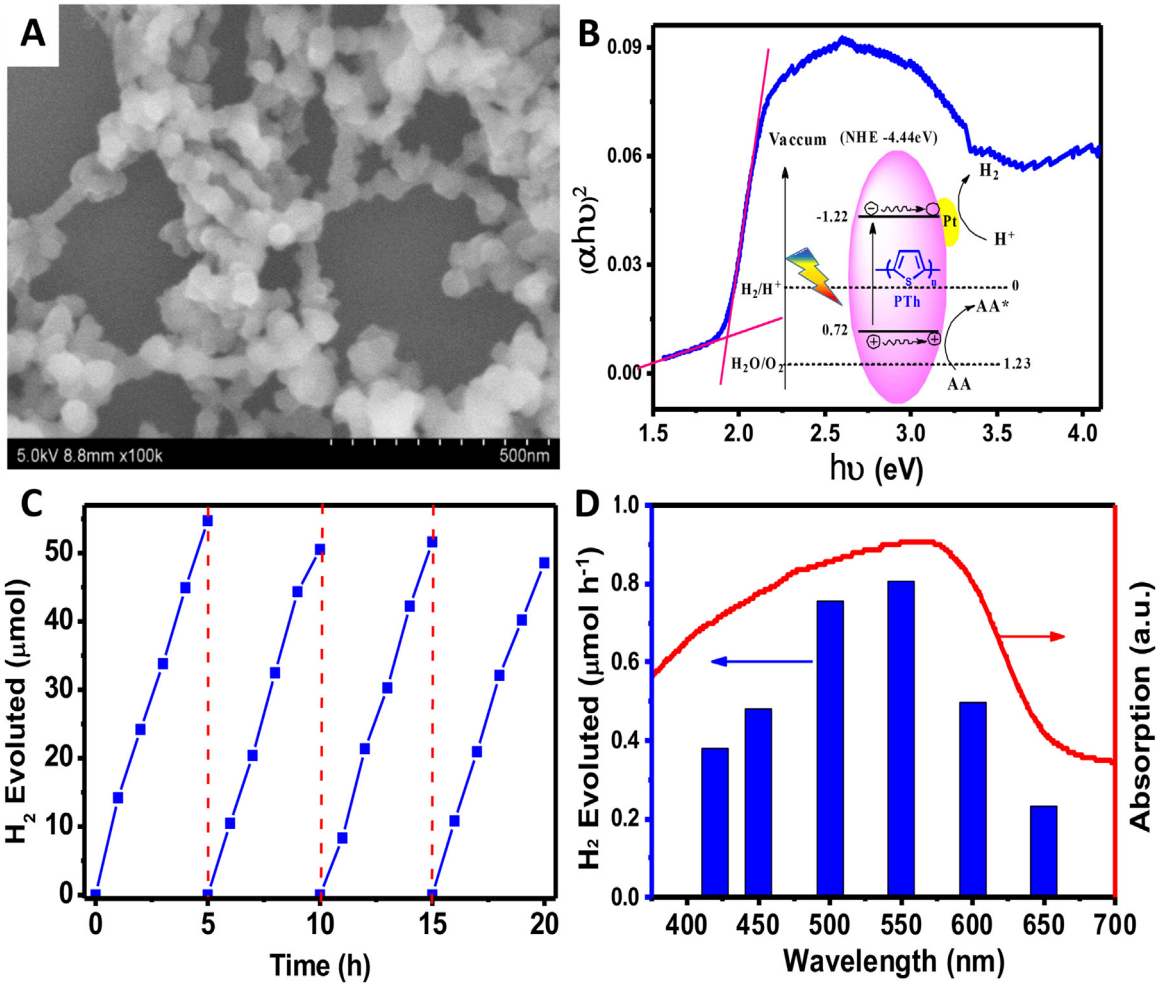

Fig. 1. (A) Scanning electron microscopy image of as-prepared PTh fiber. (B) Tauc's Plot of $(ahv)^2$ v.s. photon energy for band gap calculation of PTh fibers. Inset is the energy level diagram of PTh including the normal hydrogen reduction and water oxidation potentials. (C) H_2 production by PTh nanofibers over period of 20 h in cycles of 5 h each showing stability of PTh. Test conditions: 5 mg catalyst, 100 mL of 0.1 mol/L AA aqueous solution under 300 Xe lamp with an optical filter (λ > 420 nm). (D) DRS UV–vis spectrum of PTh nanofibers (red line). The H_2 evolution rate of PTh nanofibers under 300 Xe with different band pass optical filters with bandwidth of 20 nm. (For interpretation of the references to color in this figure legend, the reader is referred to the web version of this article.)

To illustrate that more structure defects exists in the PTh synthesized at high temperature, FTIR, Raman and ^{13}C NMR were used for the characterization. Figs. 2C and S8 show the FT-IR spectra of PTh-n (n = 0, 20 and 50). According to Yamamoto's report [39], the most intense band at 788 cm^{-1} (C_β-H out-of-plane vibration band) indicates α, α'-coupling is the dominative form of C—C bonding in all the PTh samples, whereas the small peaks at 823 and 738 cm^{-1} (two C_α-H out-of-plane vibration bands) confirm the presence of α, β'-coupling. With the increase of reaction temperature, the intensity of peaks at 737 and 820 cm^{-1} turns strength, indicating that the relative amount of α, β'-coupling increases. The Raman measurements were conducted at an excitation wavelength of 514 nm. The spectra were normalized at 1037 cm^{-1} which is a characteristic band of C_β-H bending appeared when thiophene units are α, α'-linked (Fig. 2D) [40–42]. The strongest peak observed at ~1453 cm^{-1} is attributed to symmetric in-phase vibration of thiophene rings. The intensity ratio of peaks at 1037 and 1453 cm^{-1} is associated with the content of α, α'-coupling in the polymer decreases with the polymerization temperature. At the same intensity of peak at 1037 cm^{-1}, the intensity of peak at 1450 cm^{-1} is higher in the PTh-50. It suggests that PTh-50 samples have more α, β'-coupling as the polymerization temperature increased. ^{13}C NMR spectra were also carried out, two chemical shifts at ~124.5 and 135.5 ppm were observed (Fig. 2E). It is indicative that two types of carbon exist in the conjugative polymer chain [43,44]. Normalized at the peak of 135.5 ppm, the valley at ~129 ppm raises up more than the peak at 124.5 ppm, implying that there is a peak underneath the overlap of two peaks. It is corresponding with the increased carbon signal on terminal thiophene units. The polymer chain turns short as the polymerization temperature raised. In other words, there exist more the reaction initiator center at high reaction temperature, the polymer chain number naturally increase. These results indicate that there exist more structure defects in the PTh synthesized at high temperature.

Fig. S9 shows the photographs of 5 mg of PTh-n dispersed into 100 mL water at same conditions. PTh-0 dispersion exhibits the deepest color – dark red, and the color of PTh-n samples sequentially turns lighter and lighter. It implies that the adsorption band of PTh-0 should be broader than that of PTh-50. UV–vis diffuse reflection spectra of PTh-n are illustrated in Fig. 3A. PTh exhibits a broad adsorption band in the visible light region. It should be noted the adsorption at ~585 nm significant enhanced at low the polymerization temperature. According to the previous reports [45,46], this adsorption band is related to the rod-like (π-π stacking) conformation of polymer chains in P3HT. That means that the polymer chain tends to planar arrangement through π-π stacking interaction. When the reaction occurs at low temperature, the reaction rate and reaction active center are in low state, the thiophene unit can

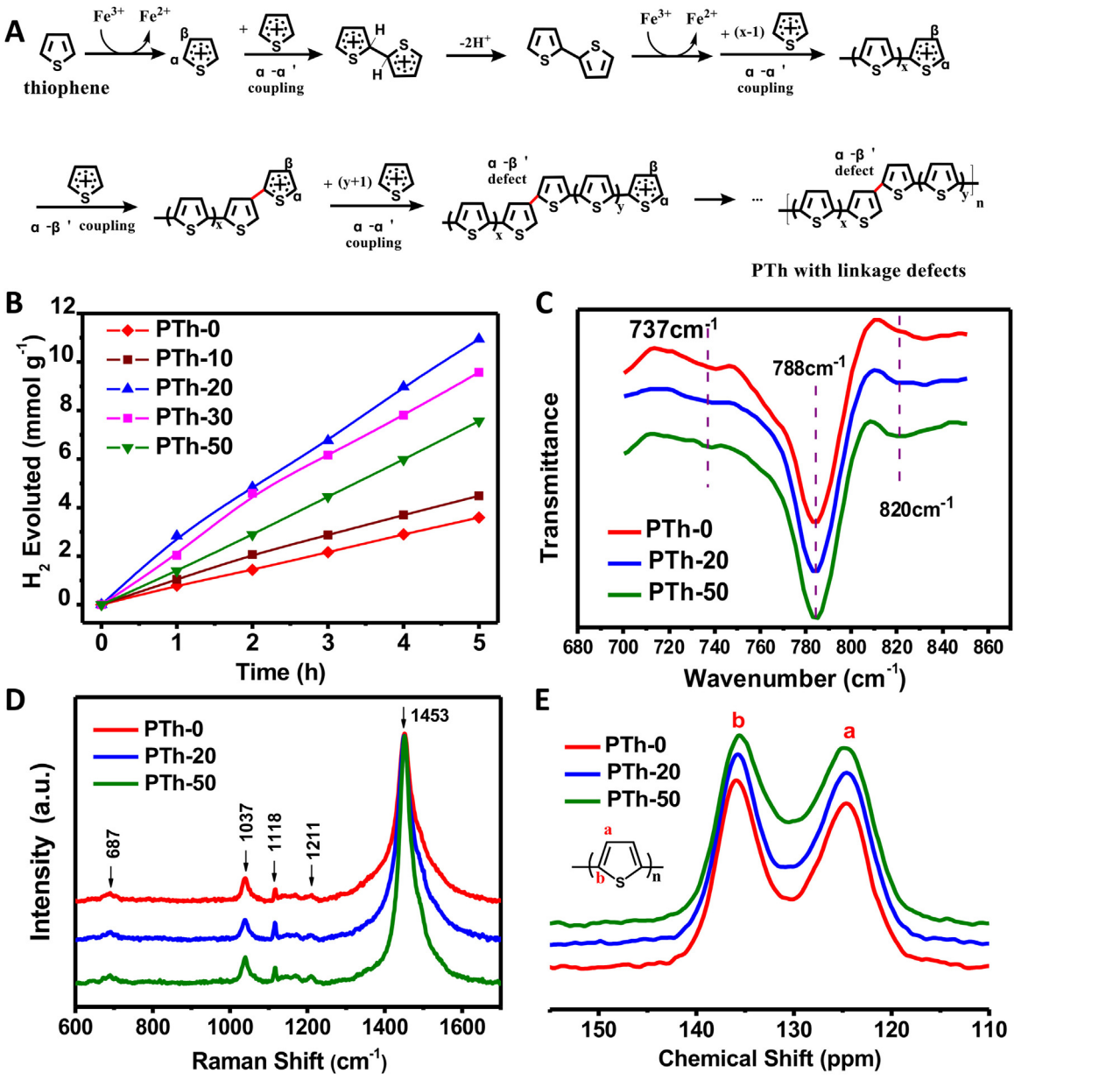

Fig. 2. (A) Schematic polymerization route to show α–α' coupling and α β' coupling of thiophene units. (B) The H2 production of PTh prepared at different reaction temperature. FTIR (C), Raman (D) and ^{13}C NMR (E) spectra of PTh prepared at 0, 20 and 50 °C.

arrange in the lowest energy way. So, the polymer chain tends to form rod-like conformation. When the reaction temperature raising, the molecular unit has more kinetic energy and more reaction center, which results in short polymer chain and coil-like conformation. The shift of π-π* transition absorption peaks to higher wavelength indicates a decreasing density of conformation, equivalent to increasing planarity, and cause gain of conjugation. Besides that, we also measure the optical extinction spectra of PTh-n water dispersion. PTh-0 not only shows strong absorption at 600 nm, but also shows strong band tail in the λ > 600 nm region (Fig. S10). That may be caused by particles scattering, which will enhance the light absorption. In the view of light absorption, PTh-0 has strongest absorption, and the PTh-50 has weakest absorption. The Powder X-ray diffraction (XRD) patterns of PTh-n (Fig. 3B) shows a broad scattering band with a peak at 24.6° related to the distance of 0.361 nm. It is associated to the π-π stacking of PTh chains [47]. Comparing all patterns, there exists a shoulder peak at ~19°, which gradually turns weak with increasing the temperature. There may exist more ordered structure in the PTh synthesized at low temperature. It confirms that the chemical synthesized PTh is mainly amorphously stack with some small ordered domain.

Based on the above analysis, the defect concentration tends to increase with increasing the reaction temperature. On the basis of inorganic semiconductor, certain amount of defects will improve the charge separation and transfer, excess amount defects inversely depress the photocatalytic activity [22–24]. Fig. 3D–F displays that TEM images of PTh-0, 20 and 50 photodeposited Pt nanoparticles under visible light irradiation for 1 h. Pt nanoparticles could hardly be found on the surface of PTh-0 sample. Then Pt nanoparticles amount gradually increases with the rise of the polymerization temperature. There are more Pt nanoparticles on the PTh-50 samples and the Pt nanoparticle size in PTh-50 is smaller than that in PTh-20. These results indicate that PTh-50 has more active sites and better charge separation due to it has more structure defect on the

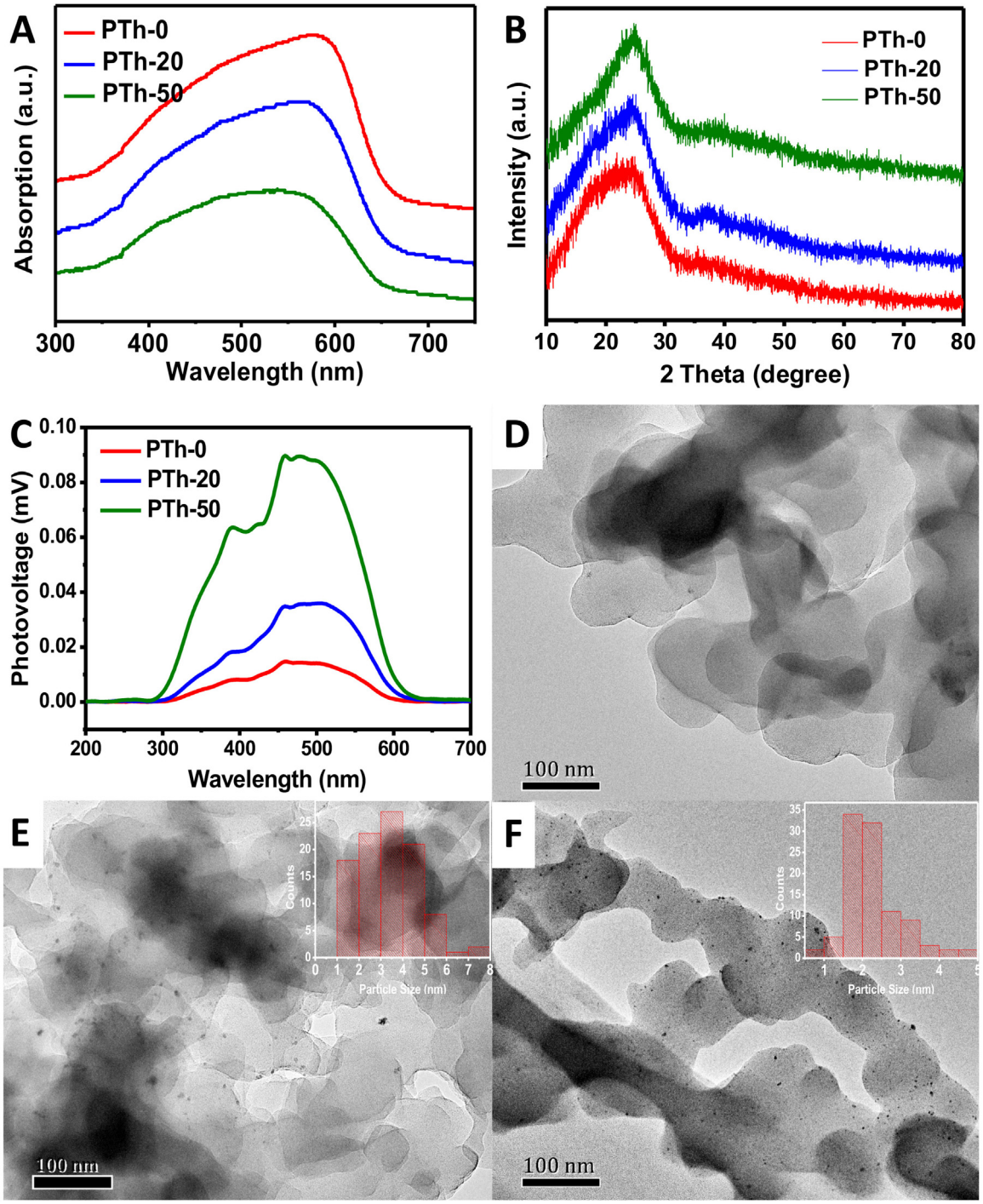

Fig. 3. DRS UV–vis spectra (A), X-ray diffraction patterns (B) and surface photovoltage spectra (C) of PTh-n prepared at different temperature. Transmission electron microscopy images of PTh-0 (D), 20 (E) and 50 (F) photodeposited Pt nanoparticles under visible light for 1 h.

PTh-50 sample. Further surface photovoltage spectra of PTh-n were shown in Fig. 3C. It shows stronger photovotage response, indicating that PTh-50 sample has best charge separation efficiency and gradually decrease with the polymerizeation temperature lower. We surmised that structure defects may stop the electron transfer and trap electron as active site because electron easily transfer along conjugated polymer chain. Overall, PTh synthesized at low temperature has more ordered π-π stacking and long conjugation length, thus it has better light adsorption. On the contrary, polymerization at high temperature results in more structure defects, which can promote charge separation efficiency. Combining both effect together, PTh-20 gives the optimum photocatalytic performance.

Based on these understandings, we designed a compound PTh photocatalyst synthesized via one-pot polymerization at different temperature. Fig. 4A shows the synthesis strategy of compound PTh fibers. Firstly, the polymerization was initiated at low temperature (0 °C) to form PTH fibers with less structure defects and better light absorption, and then raise up the reaction temperature to 50 °C to obtain the sheath layer on the PTh fibers with more defects and more active sites. We expect that the "core/shell" struc-

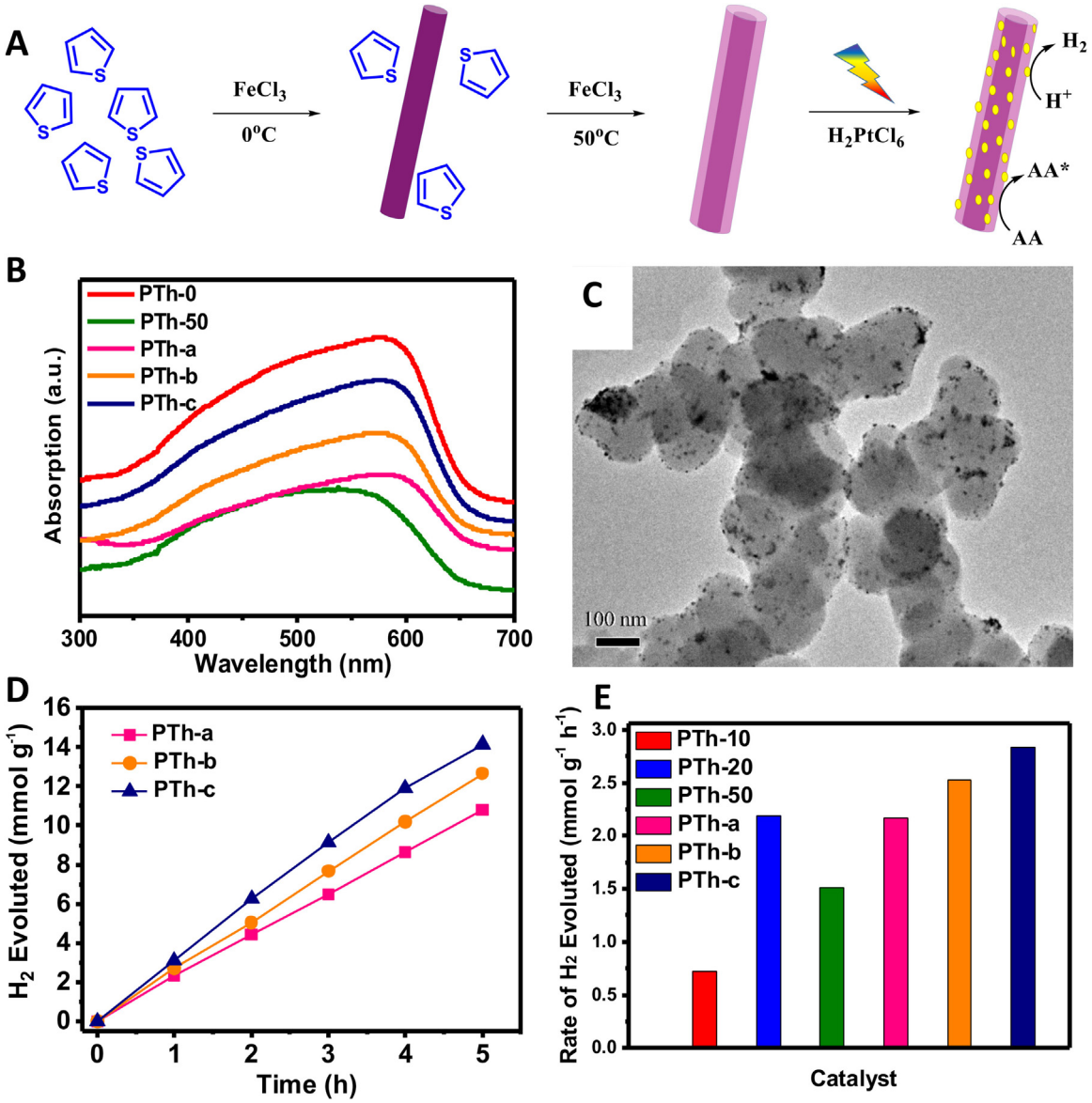

Fig. 4. (A) Schematic synthesis route of PTh compound nanofibers. PTh-a: 0 °C for 2 h and 50 °C for 3 h; PTh-b: 0 °C for 3 h and 50 °C for 2 h and PTh-c: 0 °C for 4 h and 50 °C for 1 h. (B) DRS UV–vis spectra of PTh, the reaction time of PTh-0 and 50 is 5 h. (C) TEM image of PTh-c after 5 h' photocatalytic reaction under visible light with 1.0 wt% Pt addition. (D) H_2 production and (E) H_2 production rate of PTh compound nanofibers under visible light irradiation (λ > 420 nm).

ture PTh fibers combine the light absorption of PTh-0 and charge separation efficiency of PTh-50 and give a better photocatalytic performance. PTh-a, b, c compound fibers were prepared at different reaction temperature combinations, where, PTh-a for 0 °C for 2 h and 50 °C for 3 h, PTh-b for 0 °C for 3 h and 50 °C for 2 h and PTh-c for 0 °C for 4 h and 50 °C for 1 h, respectively. Fig. 4B shows the DRS UV–vis spectra of PTh-a, b, and c and PTh-0 and 50. PTh-a, b, and c all display similar adsorption band as PTh-0, indicating PTh-a, b and c have good adsorption as our expectation. Fig. 4C illustrates the TEM image of PTh-c photo-deposited with 1 wt% Pt nanoparticles. Numerous Pt nanoparticles were deposited on the PTh fibers like PTh-50. The above results indicate more active sites were introduced on the PTh fiber by polymerizing at high temperature. Photocatalytic H_2 production of PTh-a, b, c was investigated in the 0.1 M ascorbic acid aqueous solution under visible light (λ > 420 nm) irradiation. Fig. 4D and E illustrates that all PTh-a, b, c exhibit stable H_2 Production. All compound PTh fibers exhibit better H_2 prodution rate than any single PTh-0, 20 or 50. In the compound PTh fibers, the H_2 production rate increases with the increase of polymerization time at 0 °C and decrease of polymerization time at high temperature. Among them, PTh-c displays the best H_2 prodction rate of 2.8 mmol h^{-1} g^{-1}. All these results confirm our hypothesis – PTh-0 has less structure defects and better order structure, resulting in good light adsorption. PTh-50 has more structure defects and more active site for enhancing charge separation and photocatalytic activity.

In summary, traditional linear conjugated polymer – polythiophene – could be employed as photocatalyst with excellent stability under visible light irradiation by introducing certain structure defects to promote the charge separation. Ordered polymer chain arrangement will beneficial to the light adsorption, not good for charge separation. Structure defects like α, β'-coupling, end unit or short polymer chains play a crucial role in promoting charge separation. Considering both light adsorption and charge separation, certain amount of structure defects will improve the charge separation and transfer, excess amount defects weaken the light

absorption of conjugative polymer, thus, inversely depresses its photocatalytic activity. PTh core/shell nanostructure was rational designed by take into account both light adsorption and charge separation. Two-stage temperature control polymerization was developed to obtain PTh compound nanofibers with higher reaction activity by controlling the defects amounts in bulk and on the surface of nanowires. The photocatlytic activity greatly match to our design. That may open a door to conjugated polymer for photocatalytic H_2 production.

Author contributions

All authors have given approval to the final version of the manuscript.

Acknowledgments

This work is supported by the National Natural Science Foundation of China (21671011). Z.S. thanks Beijing High-level Talent program for support. X.L. thanks financial support from the State Key Laboratory of Luminescence and Applications.

Appendix A. Supplementary data

Supplementary data associated with this article can be found, in the online version, at http://dx.doi.org/10.1016/j.apcatb.2017.04.033.

References

[1] R. Asahi, T. Morikawa, T. Ohwaki, K. Aoki, Y. Taga, Visible-light photocatalysis in nitrogen-doped titanium oxides, Science 293 (2001) 269–271.
[2] J.H. Park, S. Kim, A.J. Bard, Novel carbon-doped TiO2 nanotube arrays with high aspect ratios for efficient solar water splitting, Nano Lett. 6 (2006) 24–28.
[3] R. Konta, T. Ishii, H. Kato, A. Kudo, Photocatalytic activities of noble metal ion doped SrTiO3 under visible light irradiation, J. Phys. Chem. B 108 (2004) 8992–8995.
[4] N. Bao, L. Shen, T. Takata, K. Domen, Self-templated synthesis of nanoporous CdS nanostructures for highly efficient photocatalytic hydrogen production under visible light, Chem. Mater. 20 (2008) 110–117.
[5] H. Yan, J. Yang, G. Ma, G. Wu, X. Zong, Z. Lei, J. Shi, C. Li, Visible-light-driven hydrogen production with extremely high quantum efficiency on Pt–PdS/CdS photocatalyst, J. Catal. 266 (2009) 165–168.
[6] K. Schwinghammer, B. Tuffy, M.B. Mesch, E. Wirnhier, C. Martineau, F. Taulelle, W. Schnick, J. Senker, B.V. Lotsch, Triazine-based carbon nitrides for visible-light-driven hydrogen evolution, Angew. Chem. Int. Ed. 52 (2013) 2435–2439.
[7] K. Kailasam, J. Schmidt, H. Bildirir, G. Zhang, S. Blechert, X. Wang, A. Thomas, Room temperature synthesis of heptazine-based microporous polymer networks as photocatalysts for hydrogen evolution, Macromol. Rapid Commun. 34 (2013) 1008–1013.
[8] M.G. Schwab, M. Hamburger, X. Feng, J. Shu, H.W. Spiess, X. Wang, M. Antonietti, K. Müllen, Photocatalytic hydrogen evolution through fully conjugated poly (azomethine) networks, Chem. Commun. 46 (2010) 8932–8934.
[9] L. Stegbauer, K. Schwinghammer, B.V. Lotsch, A hydrazone-based covalent organic framework for photocatalytic hydrogen production, Chem. Sci. 5 (2014) 2789–2793.
[10] J. Bi, W. Fang, L. Li, J. Wang, S. Liang, Y. He, M. Liu, L. Wu, Covalent triazine-based frameworks as visible light photocatalysts for the splitting of water, Macromol. Rapid Commun. 36 (2015) 1799–1805.
[11] V.S. Vyas, F. Haase, L. Stegbauer, G. Savasci, F. Podjaski, C. Ochsenfeld, B.V. Lotsch, A tunable azine covalent organic framework platform for visible light-induced hydrogen generation, Nat. Commun. 6 (2015).
[12] J. HoonáPark, K. ChuláKo, J. Ko, S. MoonáLee, H. JináKim, T. KyuáAhn, J. YongáLee, S. UkáSon, Microporous organic nanorods with electronic push–pull skeletons for visible light-induced hydrogen evolution from water, J. Mater. Chem. A 2 (2014) 7656–7661.
[13] R.S. Sprick, B. Bonillo, R. Clowes, P. Guiglion, N.J. Brownbill, B.J. Slater, F. Blanc, M.A. Zwijnenburg, D.J. Adams, A.I. Cooper, Visible-light-driven hydrogen evolution using planarized conjugated polymer photocatalysts, Angew. Chem. Int. Ed. 55 (2016) 1792–1796.
[14] R.S. Sprick, B. Bonillo, M. Sachs, R. Clowes, J.R. Durrant, D.J. Adams, A.I. Cooper, Extended conjugated microporous polymers for photocatalytic hydrogen evolution from water, Chem. Commun. 52 (2016) 10008–10011.
[15] L. Li, Z. Cai, Q. Wu, W.-Y. Lo, N. Zhang, L.X. Chen, L. Yu, Rational design of porous conjugated polymers and roles of residual palladium for photocatalytic hydrogen production, J. Am. Chem. Soc. (2016).
[16] G. Zhang, Z.-A. Lan, X. Wang, Conjugated polymers: catalysts for photocatalytic hydrogen evolution, Angew. Chem. Int. Ed. 55 (2016) 15712–15727.
[17] S. Yanagida, A. Kabumoto, K. Mizumoto, C. Pac, K. Yoshino, Poly (p-phenylene)-catalysed photoreduction of water to hydrogen, J. Chem. Soc. Chem. Commun. (1985) 474–475.
[18] T. Shibata, A. Kabumoto, T. Shiragami, O. Ishitani, C. Pac, S. Yanagida, Novel visible-light-driven photocatalyst. Poly (p-phenylene)-catalyzed photoreductions of water, carbonyl compounds, and olefins, J. Phys. Chem. 94 (1990) 2068–2076.
[19] H. Yan, Y. Huang, Polymer composites of carbon nitride and poly (3-hexylthiophene) to achieve enhanced hydrogen production from water under visible light, Chem. Commun. 47 (2011) 4168–4170.
[20] Q. Zhou, G. Shi, Conducting polymer-based catalysts, J. Am. Chem. Soc. 138 (2016) 2868–2876.
[21] J. Peng, W. Gao, B.K. Gupta, Z. Liu, R. Romero-Aburto, L. Ge, L. Song, L.B. Alemany, X. Zhan, G. Gao, S.A. Vithayathil, B.A. Kaipparettu, A.A. Marti, T. Hayashi, J.-J. Zhu, P.M. Ajayan, Graphene quantum dots derived from carbon fibers, Nano Lett. 12 (2012) 844–849.
[22] H. Tan, Z. Zhao, M. Niu, C. Mao, D. Cao, D. Cheng, P. Feng, Z. Sun, A facile and versatile method for preparation of colored TiO 2 with enhanced solar-driven photocatalytic activity, Nanoscale 6 (2014) 10216–10223.
[23] H. Tan, Z. Zhao, W. -b. Zhu, E.N. Coker, B. Li, M. Zheng, W. Yu, H. Fan, Z. Sun, Oxygen vacancy enhanced photocatalytic activity of pervoskite SrTiO3, ACS Appl. Mater. Interfaces 6 (2014) 19184–19190.
[24] Z. Zhao, X. Zhang, G. Zhang, Z. Liu, D. Qu, X. Miao, P. Feng, Z. Sun, Effect of defects on photocatalytic activity of rutile TiO2 nanorods, Nano Res. 8 (2015) 4061–4071.
[25] B.R. Saunders, M.L. Turner, Nanoparticle–polymer photovoltaic cells, Adv. Colloid Interface Sci. 138 (2008) 1–23.
[26] Z. Mou, Y. Dong, S. Li, Y. Du, X. Wang, P. Yang, S. Wang, Eosin Y functionalized graphene for photocatalytic hydrogen production from water, Int. J. Hydrogen Energy 36 (2011) 8885–8893.
[27] X. Zhang, B. Peng, S. Zhang, T. Peng, Robust wide visible-light-responsive photoactivity for H2 production over a polymer/polymer heterojunction photocatalyst: the significance of sacrificial reagent, ACS Sustain. Chem. Eng. 3 (2015) 1501–1509.
[28] Y. Zhang, J. Liu, G. Wu, W. Chen, Porous graphitic carbon nitride synthesized via direct polymerization of urea for efficient sunlight-driven photocatalytic hydrogen production, Nanoscale 4 (2012) 5300–5303.
[29] J. Sun, J. Zhang, M. Zhang, M. Antonietti, X. Fu, X. Wang, Bioinspired hollow semiconductor nanospheres as photosynthetic nanoparticles, Nat. Commun. 3 (2012) 1139.
[30] M. Shalom, S. Inal, C. Fettkenhauer, D. Neher, M. Antonietti, Improving carbon nitride photocatalysis by supramolecular preorganization of monomers, J. Am. Chem. Soc. 135 (2013) 7118–7121.
[31] Y.-S. Jun, J. Park, S.U. Lee, A. Thomas, W.H. Hong, G.D. Stucky, Three-dimensional macroscopic assemblies of low-dimensional carbon nitrides for enhanced hydrogen evolution, Angew. Chem. 125 (2013) 11289–11293.
[32] J. Zhang, M. Zhang, C. Yang, X. Wang, Nanospherical carbon nitride frameworks with sharp edges accelerating charge collection and separation at a soft photocatalytic interface, Adv. Mater. 26 (2014) 4121–4126.
[33] Y. Zheng, L. Lin, X. Ye, F. Guo, X. Wang, Helical graphitic carbon nitrides with photocatalytic and optical activities, Angew. Chem. Int. Ed. 53 (2014) 11926–11930.
[34] G. Zhang, M. Zhang, X. Ye, X. Qiu, S. Lin, X. Wang, Iodine modified carbon nitride semiconductors as visible light photocatalysts for hydrogen evolution, Adv. Mater. 26 (2014) 805–809.
[35] D.J. Martin, K. Qiu, S.A. Shevlin, A.D. Handoko, X. Chen, Z. Guo, J. Tang, Highly efficient photocatalytic H2 evolution from water using visible light and structure-controlled graphitic carbon nitride, Angew. Chem. Int. Ed. 53 (2014) 9240–9245.
[36] M. Zhang, X. Wang, Two dimensional conjugated polymers with enhanced optical absorption and charge separation for photocatalytic hydrogen evolution, Energy Environ. Sci. 7 (2014) 1902–1906.
[37] Y. Hou, A.B. Laursen, J. Zhang, G. Zhang, Y. Zhu, X. Wang, S. Dahl, I. Chorkendorff, Layered nanojunctions for hydrogen-evolution catalysis, Angew. Chem. Int. Ed. 52 (2013) 3621–3625.
[38] K. Kailasam, J.D. Epping, A. Thomas, S. Losse, H. Junge, Mesoporous carbon nitride-silica composites by a combined sol-gel/thermal condensation approach and their application as photocatalysts, Energy Environ. Sci. 4 (2011) 4668–4674.
[39] T. Yamamoto, K. -i. Sanechika, A. Yamamoto, Preparation and characterization of poly (thienylene) s, Bull. Chem. Soc. Jpn. 56 (1983) 1497–1502.
[40] Y. Furukawa, M. Akimoto, I. Harada, Vibrational key bands and electrical conductivity of polythiophene, Synth. Met. 18 (1987) 151–156.
[41] E. Bazzaoui, G. Levi, S. Aeiyach, J. Aubard, J. Marsault, P. Lacaze, SERS spectra of polythiophene in doped and undoped states, J. Phys. Chem. 99 (1995) 6628–6634.
[42] C. Yong, Q. Renyuan, IR and Raman studies of polythiophene prepared by electrochemical polymerization, Solid State Commun. 54 (1985) 211–213.

[43] S. Hotta, T. Hosaka, W. Shimotsuma, 13C NMR spectrum analysis of electrochemically prepared polythienylene films, J. Chem. Phys. 80 (1984) 954–956.
[44] J. Chen, J. Shu, S. Schobloch, A. Kroeger, R. Graf, R. Mun˜oz-Espií, K. Landfester, U. Ziener, A new design strategy for the synthesis of unsubstituted polythiophene with defined high molecular weight, Macromolecules 45 (2012) 5108–5113.
[45] O. Inganäs, W.R. Salaneck, J.E. Österholm, J. Laakso, Thermochromic and solvatochromic effects in poly(3-hexylthiophene), Synth. Met. 22 (1988) 395–406.
[46] O.Y. Weng, A. Irie, H. Otsuka, S. Sasaki, N. Yagi, M. Sato, T. Koganezawa, A. Takahara, Molecular Aggregation States of Imogolite/P3HT Nanofiber Hybrid, 2011, pp. pp 012021.
[47] Z. Mo, K. Lee, Y. Moon, M. Kobayashi, A. Heeger, F. Wudl, X-ray scattering from poly (thiophene): Crystallinity and crystallographic structure, Macromolecules 18 (1985) 1972–1977.